A new pixel-wise data processing method for reflectance transformation imaging

Yuly Castro, Gaëtan Le Goïc, Hermine Chatoux, Livio De Luca, Alamin Mansouri

A new pixel-wise data processing method for Reflectance Transformation Imaging

Yuly Castro[1], Gaëtan Le Goïc[1], Hermine Chatoux[1], Livio De Luca[2], Alamin Mansouri[1]

[1] ImViA laboratory, UBFC, Dijon, 21000, France
[2] UMR 3495 CNRS/MC, Marseille, France

Abstract. Reflectance Transformation Imaging (RTI) is one of the most widely used techniques in order to digitize and analyze material appearance of a surface, finding a great level of utility and applicability in the field of cultural heritage as well as in industrial applications. To date, most of the methods used to process (model and relight) RTI data assume only one light direction for all pixels as well as a single light source-surface distance for the entire image, following the model of a very distant (far) light source. This assumption does not hold in practice. Indeed, the light sources commonly used in RTI acquisitions (spotlight / photo flash) induce to a non-uniform illumination of the surface. This is caused by the variation of incidence angles and per-point distances which directly affect the amount of light received by the surface. We propose a novel pixel-wise methodology for improving lighting based on illumination laws that allows one to correct both loss of energy due to the distance variation as well as the elevation angle. We show the efficiency of the proposed method on RTI acquisitions performed on cultural heritage objects and a manufactured surface. We show that our method corrects the effects of non-uniform illumination and leads to improve the relighting commonly associated with RTI.

Keywords: Reflectance Transformation Imaging, Illumination uniformity, Multi-light Image Collections, pixel-wise.

1 Introduction

Observing an object from a fixed viewpoint and under different lighting conditions (direction, distance, spectral range, etc.) is a widely adopted approach to analyze an object, as this provides valuable information regarding local microgeometry as well as visual appearance of the surface. Also known as Multi-Light Image Collections (MLICs), these kinds of acquisitions are commonly referred depending on the type of processing that is applied to the datasets as described in [14]. One processing strategy is the Photometric Stereo (PS) modeling approach introduced by [20], which allows one to locally determine the surface normals *i.e* pixel's orientation from the acquired images. Photometric Stereo is also widely used for estimating accurate and highly detailed 3D models by integrating the normal information [2, 5, 16].

E-mail: yuly.castro-cartagena@u-bourgogne.fr

Another known processing strategy aims to use the MLICs to reconstruct *i.e* render the visual appearance of the acquired surface; it is the Reflectance Transformation Imaging (RTI). Introduced by [8], this technique allows one to estimate the angular reflectance, which is of particular importance for the characterization of the visual appearance. Over a few years, RTI has become a widely used technique in the cultural heritage (CH) field thanks to its affordability both in terms of acquisition systems and processing of the obtained data [1, 7,11]. In addition, this technique is non-invasive, it allows to document the appearance of an object and even to create a dynamic interactive rendering of the object, which could be useful for virtual museums purposes. RTI is also a very useful method to keep track of the state of an object. The RTI technique has also been successfully developed and implemented in recent years in industrial areas for quality control of manufactured surfaces [12, 15].

Thus, MLICs have emerged as a widely utilized technique in the field of cultural heritage for studying and documenting surface appearance, offering a valuable alternative to traditional methods such as the Bidirectional Reflectance Distribution Function (BRDF) [30]. While BRDF is well-known for providing detailed information about surface characteristics like color, texture, and glossiness, its implementation requires sophisticated equipment like goniometers, spectrometers, and calibrated light sources. These instruments entail time-consuming setup and calibration processes, presenting technical challenges [31]. Moreover, BRDF measurements involve extensive computation and have limitations in angular resolution [31]. Even though some approaches have been proposed to provide a more compact representation [32], they are still excessively complex for practical application in the field of cultural heritage. In contrast, MLICs, offer a simplified approach that is particularly advantageous for cultural heritage applications.

As a part of MLICs, the RTI acquisition technique consists in acquiring a set of images of an object by a camera usually positioned orthogonal to the observed surface, while the position of the light is modified at each image capture. The information of light positions along with the corresponding images are used afterwards for relighting the surface from any arbitrary direction. This is possible thanks to fitting models transforming discrete data (acquired images and corresponding angular position) to a continuous model. To model the surface's visual appearance continuously, these discrete values can be approximated by projecting for each pixel, the vector containing the discrete measured gray-levels on a set of basis functions. This concept is illustrated in Figure 1. It can be observed in this figure the gray level values of a single pixel across the RTI dataset (same pixel across all the images). These values are modeled following three mathematical approaches. From this fitting/modeling process it is possible then to reconstruct or relight the surface appearance at any arbitrary light position. Some of the most used models to process RTI data are: Polynomial Texture Maps (PTM) [8], this approximation is a projection over a base of functions formed by the terms of a second order bi-polynomial function. The Hemispherical Harmonics (HSH) [3, 6, 17], the HSH basis is derived from a shifting of the associated Legendre polynomials and its components are expressed as functions of azimuth θ and colatitude ϕ angles over the

hemisphere in terms of l_u and l_v. The Discrete Modal Decomposition (DMD) [15], the DMD has its root in vibratory mechanics. In this method a series of a priori descriptors known as "modes" are used to create a decomposition basis named "modal basis". These modes constitute a base of elementary forms from which it is possible to describe the angular reflectance of a surface. A more recent contribution is the Principal Components and Radial Basis Functions based approach (PCA/RBF) [23], unlike the previous three methods, the RBF aims to create a new view under different light directions by using a fast and direct interpolation from a given reduced set of N multi-light images. The amount of data to be interpolated is previously reduced by the means of PCA.

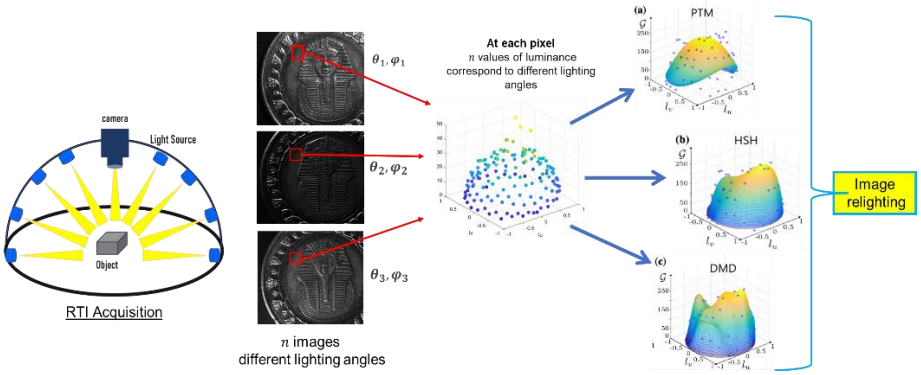

Fig. 1. Flowchart of Reflectance transformation Imaging, including acquisition, modeling, and rendering.

RTI acquisition devices can be divided into two main categories: the Dome-based [13] and the Free-form [9] methods. Two main Dome-based type of systems have been implemented. The first one employs light sources at fixed positions that are generally homogeneously distributed over the surface of the dome, and a camera at the apex of the hemisphere. In the second type, a more dynamic configuration is achieved by using a single spotlight held by an arch that can freely move over the dome to position the light to obtain the desired incident angles (azimuth and elevation). The second category (Free-form method) consists of a single light source whose position is manually moved to vary the illumination angles. This second category is the most often used for CH applications. More recently there are equipment that can be categorized as new trends in acquisition systems. Here we find systems based on robotic arms [21] and on unmanned aerial vehicles (UAV), commonly known as drones [22].

Concerning the data processing, most of the times it is considered that all the pixels of an image correspond to the same angular lighting direction and distance, which means that it considers the illumination as being collimated or that the light source is located very far compared to the scene. In this work we show that this assumption is generally not satisfied inducing significant artifacts in the results. We propose thus, a pixel-wise processing methodology that implements a point light adjustment of the illumination at each pixel, considering both the distance and the angle of incidence. We show that

thanks to the re-estimation of an angular position for each pixel, a better quality of relighting can be obtained. In this work we mainly focus on RTI technique, and the structure of the document is as follows: first we present a synthetic background of the related techniques (Section 2). Then we present the proposed methodology (Section 3). A comparison with other methods is presented in section 4. The result of applying the proposed methodology is shown in Section 5, using four datasets of RTI acquisitions corresponding to three cultural heritage objects and one manufactured surface.

2 Related works

To deal with illumination problems in MLICS some approaches have been presented. In the case of Photometric Stereo (PS) this problem has been approached and it is referred as near PS. On the other hand, in the case RTI the subject finds less contributions. Here below, we present an overview on the related works in both near PS and RTI.

2.1 PS near light methods

Iwahori et al. [24] presented one of the earliest proposals on the subject. Authors proposed a solution based on the inverse square law and the theory of monocular vision. The algorithm requires at least 4 input images and a large angle variation between images, to produce a significant difference on the illumination. Additionally, as mentioned in their work, the distance between the light source and the studied object needs to be large. These last two conditions are the main drawbacks of their method.

Quéau et al. [25] proposed a model for photometric stereo under point light source illumination, considering the nonlinearities due to distance and to the anisotropy of the LEDs. The algorithm first corrects the input images, to get a more uniform lighting. For performing the correction, the method uses an ambient light image and following the Cosine-Fourth Power Law of Illumination, creates a $COS^4\alpha$ map to compensate for darkening at the borders. Its main drawback is the need of camera intrinsic matrix to estimate the solution.

Santo et al. [26] proposed a per-point solution, in which a distant light setting needed to be considered to produce a solution. This approach is based on a deep learning algorithm, and therefore a large dataset is needed to train the model. Otherwise, a pre-trained PS network can be used, but in this case the network is pre-trained with distant assumption PS data. This method is computer dependent, takes at least half hour for processing and render a 256x256 images input dataset in a powerful computer (tested on an NVIDIA Quadro RTX 8000 GPU).

2.2 Illumination problems in RTI

Different solutions have been proposed to consider artifacts caused by near illumination in RTI approaches and applications. For instance, to address the estimation of the angular position of the incoming light in Free-form acquisitions, *Winnemoeller et al.* [19] proposed an algorithm capable of automatically extract three-dimensional light position from acquired images. This approach does not use reflective shiny spheres, but it involves the use of a diffuse reflector in addition to the light source. The method also relies on having small distances between successive angular positions in the image stack. This could be a good and applicable solution when using an automated Dome-based system, on the other hand in the case of Free-form as light is usually handheld it is difficult to accomplish small successive light positions.

Walton et al. [18] proposed a distance compensated pixel intensity framework that follows a near point illumination model in order to correct the non-uniform lighting and to estimate light directions. This method eliminates the need of placing shiny spheres, however, the method relies in the use of a flat matte surface such a color checker that needs to be placed in the scene. Their method proposed an estimation of 3D scene points but still requires initial values for combined albedo and vignetting. Initial surface normal estimates are also needed. Considering this last requirement, this methodology can be thus difficult to implement if images are acquired with non-rigorous conditions, like for H-RTI (Highlight RTI), where acquisition conditions may often lead to inaccurate normal map estimation.

More recently, *Giachetti et al.* [4] show that, with a modification of the standard acquisition setup, it is possible to significantly improve the quality and accuracy of the relighting model. This work introduces the idea of correcting the light direction and intensity using the per pixel light direction estimation from the highlights on multiple reflective reference spheres by considering perspective correction and performing direction linear interpolation. While for compensating the illumination variations the authors proposed an algorithm exploiting light intensity measured on matte white targets positioned around the object of interest. The main drawback of this method is the need of extra equipment to perform the acquisition, which implies that exiting datasets cannot be processed following this method.

McGuigan et al. [10] proposed a novel method to estimate light directions without the requirement of a calibration equipment, reference spheres and hence claim that their method can be retrofitted to any existing stack of RTI photographs. The first step in this approach is isolating intensity variations due to light source by subtracting each image with the mean image of the whole stack. Secondly, an intensity correction method is proposed. Similar to PTM, the method uses bi-quadratic functions to fit and to correct the intensities. The standard PTM method uses the bi-quadratic function to estimate the orientation of a given pixel, whereas this method fits the orientation collectively to all pixels in each image for intensity correction. The results show a particularly marked

improvement in the surface normal map estimation in comparison to the standard H-RTI method.

As for other works related to illumination in RTI acquisitions, *Castro et al,* [30] studied the impact of the non-uniform distribution of light positions in RTI acquisitions and its consequences on surface relighting. In this work, the authors investigate the distribution of lighting directions that especially in the case of H-RTI acquisitions do not end up generating a homogeneous distribution in the hemispheric space. This undoubtedly affects the reconstruction of the surface (relighting) since the methods commonly used for this task (PTM, HSH, DMD) assume said uniformity. To address this issue, the authors propose a methodology consisting in the estimation of the spatial distribution of the lighting directions used during RTI acquisitions, using an estimate of the local density. These local density values are used subsequently to weight the Least Squares regression, and thus correct the contributions of each image of the RTI acquisition.

Following these presented publications, in the case of PS application none of these solutions is easily adaptable for RTI data, that usually produces around 70 images, at different light positions to provide enough data for the relighting fitting algorithm and obtain accurate normal map estimation. In the case of RTI, the presented methods propose the estimation of the angular position of the incident light but providing only a single position for the entire surface. Only one method proposed the estimation of the angular position per pixel. However, it is based on the use of 4 reflective spheres since the method requires multiple points to create an interpolation and estimate a per-point angular position. Considering this, we propose a methodology that helps to improve illumination uniformity of the surface as well as it allows to estimate a per-pixel angular position without the need of any additional equipment or target in the acquired scene.

3 Proposed RTI data processing methodology

For a diffuse shaded surface, directly illuminated by a point light source of fixed intensity, the illumination received by the surface varies as a function of two parameters: (1) the angle between the normal surface and the light rays (the Lambert's Cosine Law) and (2) the distance from the light source (the Inverse Square Law) as illustrated in Figure 2.

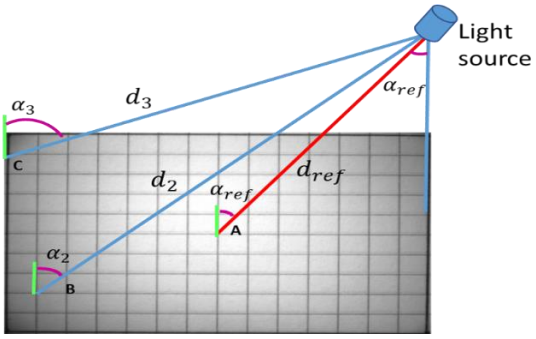

Fig. 2. With a point light source, the distance d_i and the angle α_i varies with the pixels (A to C).

Following these two illumination laws, we propose a solution to adjust the pixel value to compensate the loss of energy *i.e* loss of illumination produced by the spread of light on the surface. We also propose to use the per pixel estimated angular position, to improve and reduce inaccuracies for the RTI modeling. We present how the angular position as well as the distance can be estimated for each pixel of the image. Once these values are obtained, we use the per pixel distance information as well as the per pixel elevation angle information to estimate a pixel-wise correction coefficient to perform an illumination adjustment. Then, we show how the corrected images as well as the per pixel set of angular positions (θ, ϕ) can be used for RTI modeling and relighting steps. The proposed methodology consists of two blocks of steps: The first block (B1) can be applied to any existing dataset, while the second one implements an improvement for dark and saturated pixels, for which it is necessary to acquire a second image at the same angular position. The second block (B2) is independent from the estimation of the pixel-wise illumination obtained in the first block. The B1 of the methodology can thus be applied to pre-existing RTI datasets. The proposed method is summarized in the flowchart presented below (Figure 3).

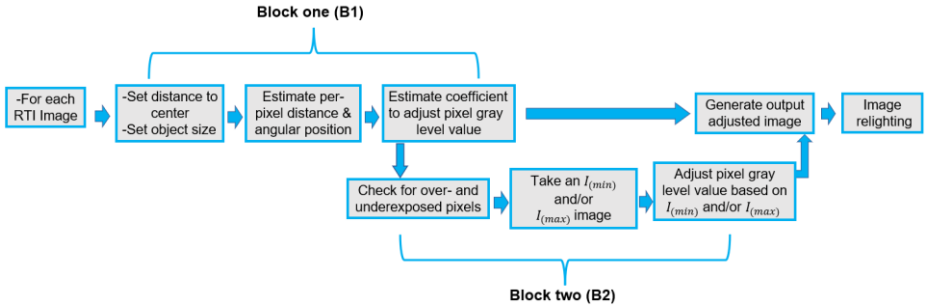

Fig. 3. Flow chart of the proposed methodology.

3.1 Pixel-wise distance, angles, and coefficients estimation (B1)

To estimate a distance and angular position (θ, ϕ) for each pixel, there are two reference values that are needed considering the standard RTI configuration presented in Figure

4. The first one is the distance between the light source and the center of the surface. The second is the angular position of the light source with respect to the center of the surface (see Figure 2 and Figure 5). From this information and knowing the real size of the surface, it is then possible to estimate a new set of distance and angular position values for each pixel. This methodology is presented below.

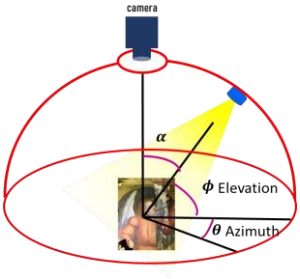

Fig. 4. Representation of the standard RTI angular position (θ, ϕ) of light source.

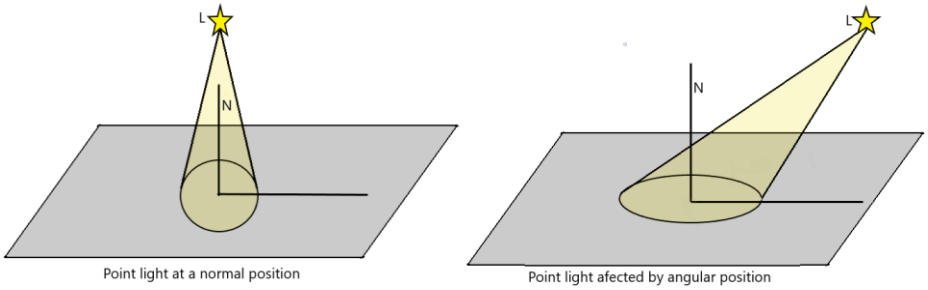

Fig. 5. Lambert's Cosine Law: For a non-collimated light source, the light scatters more when it is oriented in grazing positions with respect to the surface. Thus, for a normal position, the surface will receive the highest percentage of illumination, on the contrary, in a grazing position, the energy received will be lower, which translates into a darker image.

Step B1.1 Determine and set distance and angular reference.
At this point, the angular position of the light source and the distance between it and the center of the surface must be determined (radius of the hemisphere). This depends on the acquisition system used, which in this case is an automated dome-type system with a radius of 220 mm and known angular positions. At this stage it is also necessary to input the real size of the acquired scene.

Step B1.2 Per pixel distance and angular position estimation
Let be $P = (x_1, y_1, z_1)$ and $Q = (x_2, y_2, z_2)$ two points in the space, the distance between them is defined by:

$$d(P,Q) = \left|\left|P.Q\right|\right|_2 = \sqrt{(x_2 - x_1)^2 + (y_2 - y_1)^2 + (z_2 - z_1)^2} \quad (1)$$

The estimation of angle between two points is given by:

$$\alpha = arcos\left(\frac{P.Q}{||P||_2.||Q||_2}\right), \quad (2)$$

where $P.Q$ is the scalar product of P and Q and $||P||_2.||Q||_2$ is the product of magnitudes of P and Q.

Step B1.3 Estimation of pixel-wise adjustment coefficients

The inverse square law of illumination is given by:

$$E_{i,j}^{d} = \frac{I_{i,j}}{d_{i,j}^2}. \quad (3)$$

As shown in Figure 2, the distance d is pixel dependent. To normalize the illumination as if it was uniform, we need to adjust the illumination based on a reference distance d_{ref}.

$$E_{i,j}^{d_{ref}} = \frac{I_{i,j}}{d_{ref}^2} = K_{i,j}^{d}.E_{i,j}, \quad (4)$$

where d_{ref} is the distance of the pixel at the center of the surface. We obtain the coefficient $K_{i,j}^{d}$ by the relation:

$$K_{i,j}^{d} = \left(\frac{d_{i,j}}{d_{ref}}\right)^2. \quad (5)$$

The Lambert Cosine's Law is given by:

$$E_{i,j}^{\phi} = I_{i,j}\cos(\alpha_{i,j}), \quad (6)$$

where α is the elevation angle with respect to the normal, as shown in Figure 4. As the cosine law considers the elevation angle with respect to the normal (angle α) in order to obtain the elevation angle as used in the standard RTI model (angle ϕ) as shown in Figure 4 we must note:

$$\phi + \alpha = \frac{\pi}{2}, \quad (7)$$

Therefore

$$E^{\phi} = I\cos(\alpha) = I\sin(\phi). \quad (8)$$

With ϕ_{ref} being the elevation angle of pixel at the center of the surface $E_{i,j}^{\phi_{ref}} = I_{i,j} * \sin(\phi_{ref})$. A coefficient $K_{i,j}^{\phi}$ is obtained as follows:

$$K_{i,j}^{\phi} = \frac{\sin(\phi_{ref})}{\sin(\phi_{i,j})}. \quad (9)$$

A final coefficient to apply to each pixel of a given input image, is obtained using both coefficients previously estimated $K_{i,j}^{\phi}$ and $K_{i,j}^{d}$.

Step B1.4 Final step image adjustment

An adjusted output image (I_{s1}) is obtained following the equation:

$$I_{B1}(i,j) = (K_{i,j}).(I_{i,j}), \quad (10)$$

Where,

$$K_{i,j} = \left(K_{i,j}^{d}.K_{i,j}^{\phi}\right) = \left(\frac{d_{i,j}}{d_{ref}}\right)^2.\left(\frac{sin(\phi_{ref})}{sin(\phi_{i,j})}\right). \quad (11)$$

3.2 Validation of block of steps one (B1)

To verify the proposed methodology, we analyze the angular and distance variation of a particular angular position ($\theta = 10°, \phi = 24°$) obtained on a standard reference surface (ColorChecker GRAY BALANCE). An RTI acquisition was carried out using a dome system with a single light source held by a motorized arch. The presented surface was acquired over 77 light angular positions homogeneously distributed over the hemisphere, using a 12.4 Megapixel monochrome camera. The distance from the light source to the center of the surface is 220 mm and the acquired area is 30 x 50 mm. Figure 5a shows the variation of the estimated distance depending on the pixel. Considering that light arrives to the surface from the upper right side ($\theta = 10°, \phi = 24°$), the smaller distance values are in the right up corner ($197.5\ mm$). On the other hand, as light spreads into the surface, the larger distance is obtained at the left bottom corner pixel ($245\ mm$). This is the expected behavior, considering that the distance at the center is $220\ mm$, as the points on the surface move away from the central position, the

distance difference to the center increases. This behavior is evident by observing the diagonal of the distance map (Figure 6a).

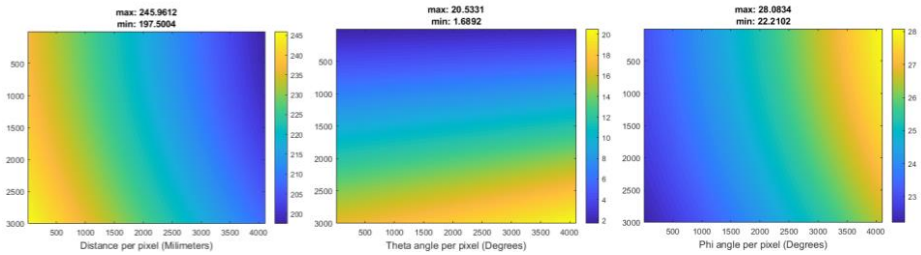

(a) Distance map *(b) θ map* *(c) ϕ map*

Fig. 6. Distance and angular(θ, ϕ) per pixel maps.

Consequently, the ϕ map presented in Figure 6c, follows an inverse relationship, as distance grows, the elevation angle decreases and vice-versa. Having a 24° elevation angle at the center of the surface, the largest angle is found in right upper corner 28° and the smallest at the down left corner 22°. As light spreads following a conical shape (solid angle), the azimuth angle also diverge from the one found at the center of the surface (10◦). The variation of this angle can be observed in Figure 6b.
Finally, we provided distance and angular variation along the first 21 images of the acquisition dataset. Figure 7a, we can see the variation of the elevation angle across all pixels of 21 images. One of the largest variations is observed at image 10, where the central angle corresponds to 37°, but the maximal and minimal values correspond to 43.4° and 32.2°, respectively. In Figure 7b the angular variation on the azimuth is shown, and one of the greatest variations is observed at image 14 where the angle at center pixel is 168.8° with a maximum of 177.6° and minimum of 158.6°. This represents a 19 % of difference.

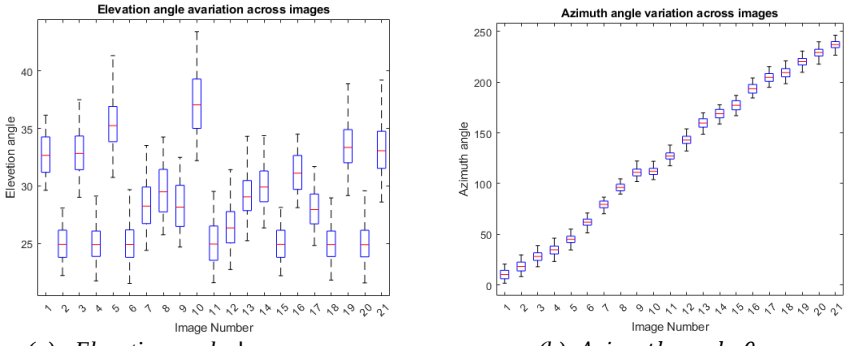

(a) Elevation angle ϕ *(b) Azimuth angle θ*

Fig. 7. Angular variation across pixels on first 21 images of the dataset ColorChecker GRAY BALANCE.

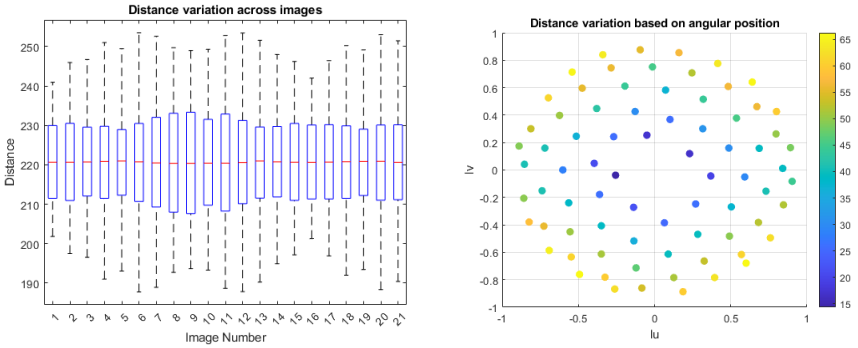

(a) Distance variation along 21 images *(b) ϕ map Distance variation along dataset according to angular position*

Fig. 8. Distance variation across pixels on images of dataset ColorChecker GRAY BALANCE.

In Figure 8a it can be seen the variation of distance for all pixels across the 21 images of the dataset. Finally on Figure 8b the percentage of distance variation for all of the 77 images of the dataset is shown, but with respect to the angular position. As it can be seen in the Figure 8b, at grazing positions, distance variation is larger, and it is smaller at angular positions closer to the normal.

3.3 Considering black and saturated pixels (B2)

In cases where there is a presence of either, saturated or black pixels, an additional adjustment coefficient should be applied. This additional process allows to improve the resulting image and to apply the coefficients acquired in B1 to unmeasured pixels (black and/or saturated). To apply this step, it will be necessary to take one or two more pictures at the same light position, depending on the following thresholds.

Step B2.1 Check for over- and underexposed pixels
For an image with gray value levels defined between 0 and 255, we define two thresholds. Consequently, for pixel values equal or less to five (≤ 5) are considered as underlit and pixel values equal or superior to two hundred fifty (≥ 250) as overlit. These thresholds were chosen considering the non-linear behavior of the camera at the borders.

Step B2.2 Take an I_{min} and/or a I_{max} image at the same angular position.

Let be K_{min} the minimum and K_{max} the maximum value of the coefficient $K_{i,j}$. When the image presents saturated pixels (overlit) a new Image I_{min} is acquired.

$$I_{min} = exposure\ time. K_{min} \qquad (12)$$

Where, the exposure time is related to lighting time of the LED as is synchronized with aperture time of the imaging sensor.

When the image presents dark pixels (underlit), a new image I_{max} is acquired

$$I_{max} = exposure\ time. K_{max} \qquad (13)$$

Step B2.3 Adjust pixel gray level value based on $I_{(min)}$ and/or $I_{(max)}$

Once an $I_{(min)}$ *and/or* $I_{(max)}$ is acquired a new output image I_{B2} can be determined adjusting for each pixel the gray level value as follows:

For every pixel $I_{i,j} \geq 250$

$$I_{B2}(i,j) = I_{min}(i,j).\ \left(\frac{K_{i,j}}{K_{min}}\right) \qquad (14)$$

For every pixel $I_{i,j} \leq 5$

$$I_{B2}(i,j) = I_{max}(i,j).\left(\frac{K_{i,j}}{K_{max}}\right) \qquad (15)$$

Thus, for pixel values withing the range of $5 \geq pixel \leq 250$, the final adjusted value depends solely on result produced at B1.

3.4 Proof of concept

In this section we present a proof of concept of the proposed methodology, we show the results obtained with the proposed correction at different light angular positions.
A test RTI dataset is obtained using a fully automated Dome-based system. The RTI acquisition was performed over a flat surface (7.5×5.8 cm), using 76 light positions ($22\ cm$ surface-light source distance). The block of steps 1 (B1) of the proposed methodology was applied to the images. Figure 12a shows the input image at light position ($\theta = 9.4°, \phi = 20°$) before applying the proposed method. First the per-pixel distance and angular position are estimated. From the distance map (Figure 9a) the distance coefficients per-pixel are estimated result can be seen in Figure 9b.

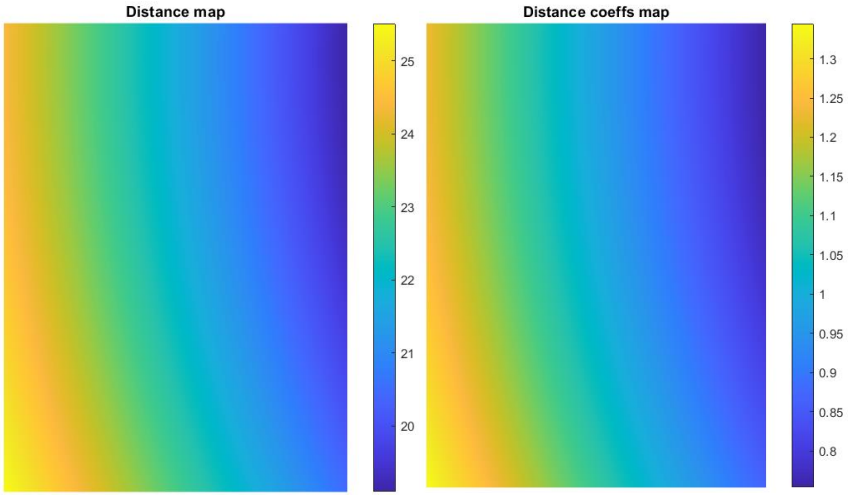

(a) Distance map *(b) Distance coefficients map*

Fig. 9. Distance and distance coefficients maps for input image at position $\theta = 9.4°, \phi = 20°$.

Then, per-pixel coefficients from the phi map (Figure 10a) are estimated. The resulting map can be observed in Figure 10b. In can be notice that light is coming from the right side of the surface, thus the higher value of the elevation (phi) angle is closer to light and this value decreases as we move to the left side. Furthermore, the coefficients map estimated from Equation 9 follows an inverse proportional relationship. Thus, for larger angles we apply a smaller coefficient and vice versa.

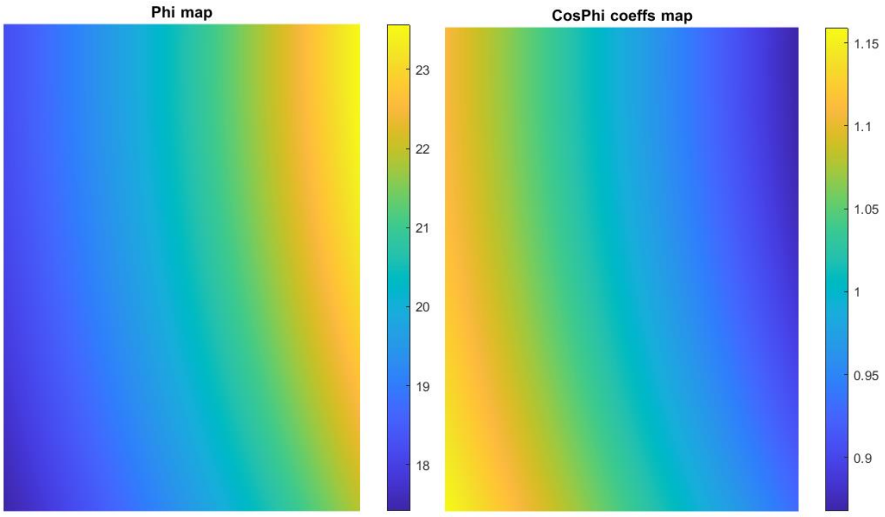

(a) Phi map *(b) Cos phi coefficients map*

Fig. 10. Phi and Cos phi coefficients maps for input image at position $\theta = 9.4°, \phi = 20°$.

The final coefficients that are applied to input image can be seen in figure 11. This coefficient is the result of combining both distance and cos phi coefficient maps.

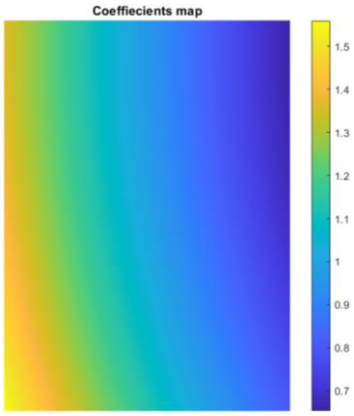

Fig. 11. Final coefficients map to apply to input image at light position $\theta = 9.4°, \phi = 20°$.

In figure 12b, the result of applying the final coefficients map to the input image can be seen. As we can observe for the input image light is stronger at the right-side coinciding with the position closest to the light source, likewise the light is dimmer on the opposite (left) side, since this part of the surface is further away from the light source. After applying the proposed methodology, we can see in the resulting image how the lighting presents a more homogeneous spreading pattern.

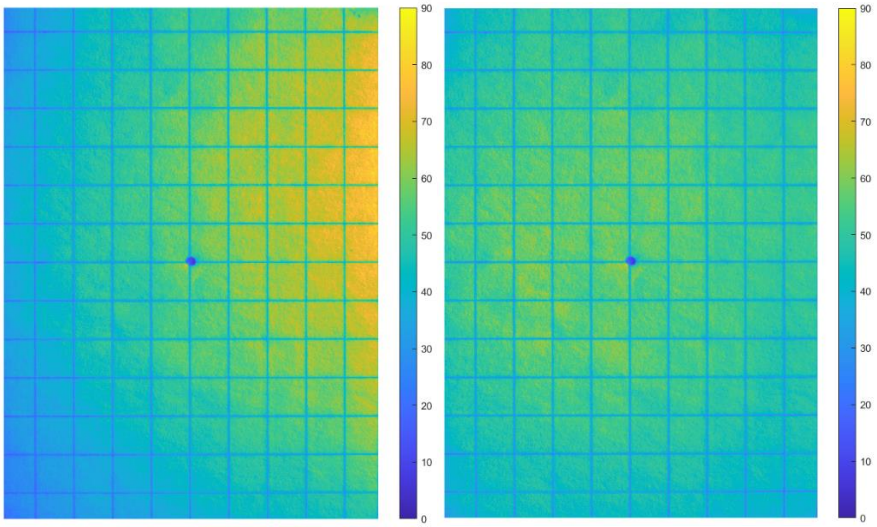

(a) Input image *(b) Corrected image*

Fig. 12. Input image at position $\theta = 9.4°, \phi = 20°$, before and after applying the proposed methodology.

In Figure 13 we present the results obtained by applying the proposed method for another angular position ($\theta = 83.74°, \phi = 29.16°$). Figure 13a shows the input image, and Figure 13b shows the resulting image after applying the proposed methodology. It can be observed in that after applying the proposed methodology the surface presents a more uniform illumination.

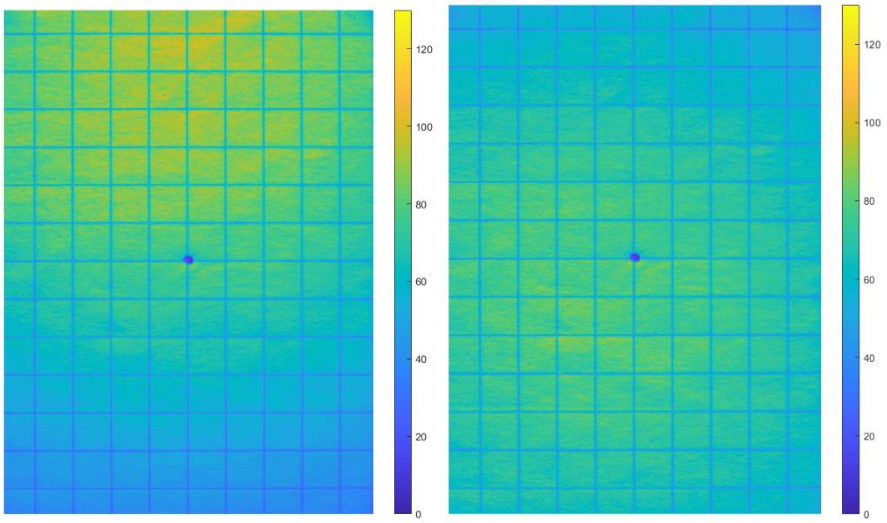

(a) Input image *(b) Corrected image*

Fig. 13. Input image at position $\theta = 83.74°, \phi = 29.16°$, before and after applying the proposed methodology.

4 Comparison methods

In this section we present the comparison of our method with the approaches presented by [4] and by [10]. These two methods have been chosen since to our knowledge they are the most recent methods that deal with a similar problem and that are specifically focused on RTI.

As far as we know, the only known approach proposing a per pixel correction of the lighting position is the one presented by *Giachetti et al*. [4]. This method described in section 2, proposed the use of four specular spheres and a matte white target positioned around the object of interest. From each sphere is possible to extract a light position file (LP file) and then implement a linear interpolation of the related information of each of the four LP files to produce a per pixel angular position correction. Additionally, with the matte surface authors proposed a correction of light uniformity, Unfortunately, given the fact that this element must be included in the scene during acquisition, it is not possible to perform a correction of this type to an already existing dataset. So here we compare the part of the method that suggests the angular correction per pixel, with our methodology which proposes another method to perform this correction.

As previously stated, one of the issues associated with RTI models is that they are based on assumptions that cannot always be satisfied. One of theme, is the way light spreads. We have explained that this is mainly influenced by two parameters linked to light distance and incident angle. As a result, it is reasonable to infer that the angular location of the light source in relation to the surface varies depending on the point at which it is evaluated. Because of this, the location relative to the surface's center will differ from the predicted position at the surface's corners. Based on this idea, an experiment was conducted employing a calibrated dome in which the angular location of the light (relative to the center of the surface) is known and reliable. A surface of $(7 \times 5cm)$ has been prepared, with four reference spheres put in the corners. An RTI acquisition was conducted. The four LP files are extracted from the test dataset using the approach described by [4]. We then take as ground truth (LPref) the angular potions of the dome. Then we choose to analyze an image of the dataset corresponding to a particular angular position. then we compare the angular position per pixel obtained with our method and the one obtained through linear interpolation as suggested by [4].
Figure 14a presents a real-color grayscale image acquired at angular position θ = 30°, ϕ = 20°. Figure 14b shows the same image using a false colormap to better visualize the intensity variation.

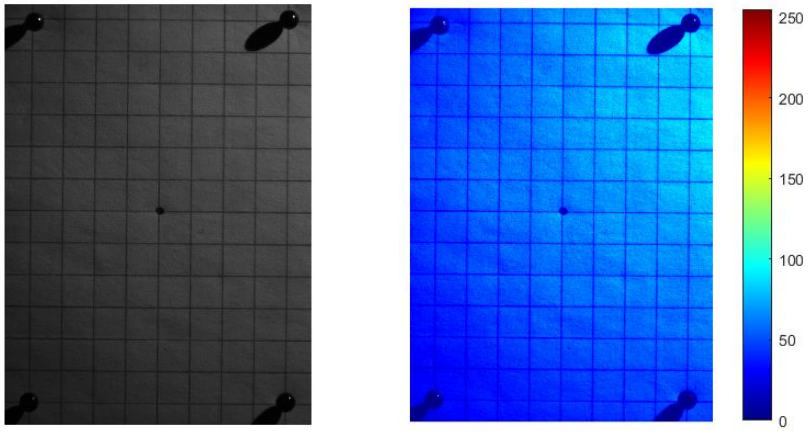

(a) Acquired image at $\theta = 30°, \phi = 20°$
(b) Acquired image at $\theta = 30°, \phi = 20°$ in false colormap

Fig. 14. Input image at position $\theta = 30°, \phi = 20°$

Image in Figure 14 shows how light reaches from the top-right corner of the surface and spreads towards the center, while its intensity decreases according to distance. The angular position measured at the center of the surface is known (dataset acquired with an automated Dome-based system) and used as ground truth. From the four spheres positioned at the corners, the angular position is estimated (by highlight detection) and then from the coordinates obtained from each sphere a linear interpolation is performed.

Figure 15a shows the rusting per pixel angle map obtained for the elevation angle (ϕ). When measuring the angle at the center of the surface from the interpolated map (indicated in the figure), it can be seen that it does not match the real angular position. In this case, the estimation presents a 2.14 error. Figure 15b, shows the result produce by the our proposed method. The estimation error of the angle measured at the center of the surface is 0.03. It can also be seen how the angle variation per pixel behaves similarly to the spread of light seen in the input image (Figure 14b). Something similar occurs with the azimuthal angle, as seen by the 15.27 difference between the linear interpolation estimate and the ground truth (see Figure 16a). In contrast, the estimate obtained using the proposed method, which only differs by 0.1 (see Figure 16b). Thus, we can see that our proposed method for estimating the angular position per pixel is closer to that produced by the propagation of light beams on the surface.

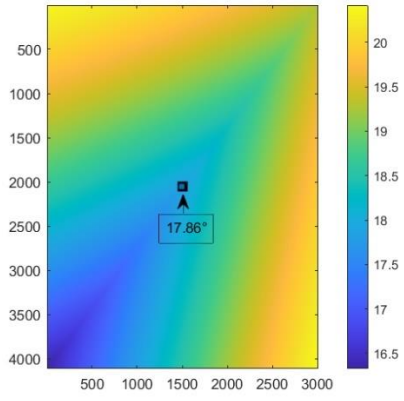

a) Elevation angle map from linear interpolation.

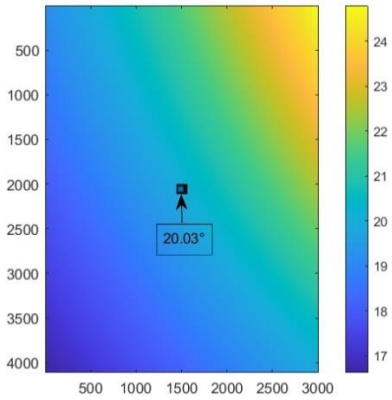

(b) Elevation angle map from proposed method.

Fig 15. Per pixel angular position variation for elevation angle (ϕ).

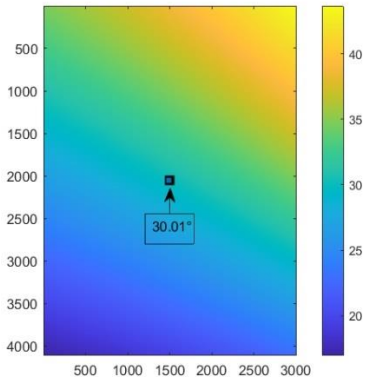

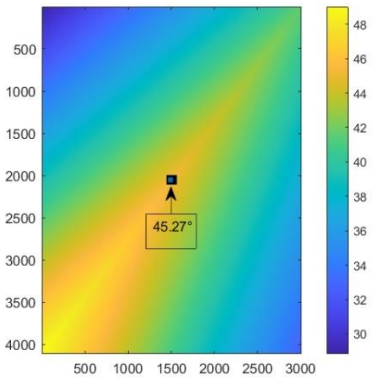

a) Azimuth angle map from linear interpolation. *(b) Azimuth angle map from proposed method.*

Fig 16. Per pixel angular position variation for azimuth angle (θ).

In the case of a homogeneous illumination, (use of a collimated light), the angular position for each point of the surface would be the same, (the value obtained in the center of the surface). From this we can deduce that in our method, if the surface were homogeneously illuminated, the application of the proposed correction would not produce any alteration in the illumination of the surface since the correction coefficient obtained according to equations 5 and 9 would be 1.

Here we compare our proposed method, with the one introduced by *McGuigan et al.* [10]. As explained in section 2, this method provides a way to estimate the light direction without the need for specular speres and it also proposed a methodology for correcting non uniform illumination in RTI images. Here we compare this last approach. As described by the authors, for each image (I), in the image stack they generate mean-corrected version of the image (Ic). Then fit a bi-quadratic function to the lighting intensity across Ic. And finally, use the fitted function to compensate for over-lit and under-lit regions. In Figure 17, we show the results obtained with this method when applied to input image in angular position $\theta = 30°, \phi = 20°$ (Figure 17a).

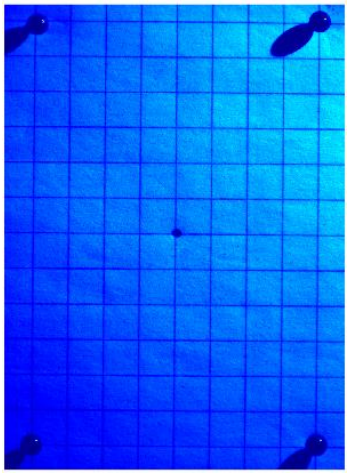

a) Input image

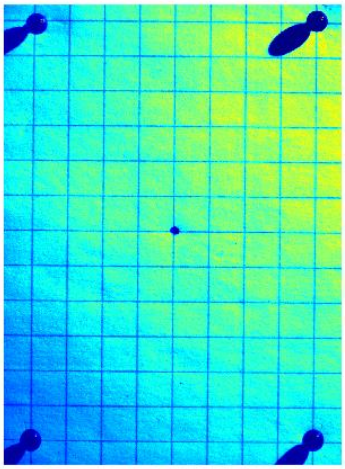

b) Inverse of function fitted to light variation in (a)

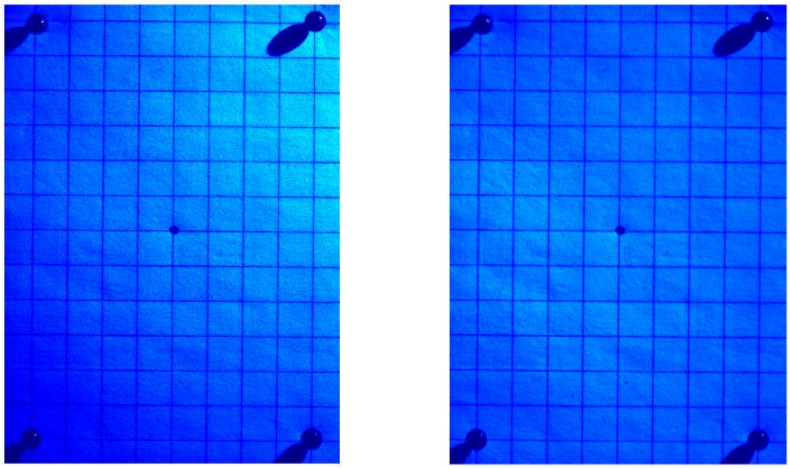

c) Intensity correction generated by the method proposed in [10].

d) Intensity correction generated by our proposed method.

Fig 17. Intensity correction generated by the method proposed by [10] compared to the result optained with our proposed method.

As can be seen in Figure 17c and as the authors directly specify in [10], the intensity correction produced is subtle, since according to what they explain, the non-uniformity of the lighting should not be over-corrected as it could have an effect on noise amplification. In Figure 17d we can see the result that is obtained for the input image (Figure 17a), using our proposed method. Here, it can be seen that the light intensity is no longer concentrated in the top-right corner of the surface, but instead thanks to the correction, the light diffuses more evenly on the surface.

5 Application on CH and manufactured objects

In this section, two cultural heritage (CH) and a manufactured objects are used to show the improvement brought by the proposed method. The first dataset was obtained using the SyntheticRTI, a plugin that allows one to created Multi-light Image Collections using the Blender rendering engine. The render object is a 19th century headstone standing of Monsea church ruins, Co. Tipperary, the model can be download from SketchFab (https://sketchfab.com). The render area can be seen in Figure 18a (red rectangle). The second one (dataset RTI-D2, Figure 18b), is a modern daguerreotype made by Marinus Ortelee. This object was acquired using and automated Dome-based system. The size of the object is $42.9 \times 28.8\, mm$. The third dataset (RTI-D3, Figure 18c) is an H-RTI acquisition that was made on a part of a famous historical painting named Retable de la Trinité (Catalan school), a painting on wood attributed to Canapost's Master (XVth century) and located at the Hyacinthe Rigaud museum of arts in Perpignan, France. The size of the artwork is 3,69 m. height and 2,19 m wide, but the acquisition zone corresponds to $0.297 \times 0.21 mm$ (marked with the blue rectangle). This

third dataset is used to show the results regarding RTI relighting after the B1 of the proposed correction is applied to the input image. The image is relighted using the per-pixel light positions (θ, ϕ), estimated as shown in *Step B1.2*. The RTI acquisition was carried out during a restoration process of the artwork. This allows keeping a record of the state of the artwork before restoration. H-RTI acquisitions often lead to inaccuracies during the surface modeling, as some requirements regarding the acquisition are difficult to fulfill, such us keeping a constant distance between consecutive images or properly pointing light to the center of the surface. Even if one gets to manage these aspects, the correction of non-uniform illumination is necessary when it comes to acquiring large-scale objects. The effects generated by the illumination must be considered during data processing to avoid artifacts during the reconstruction *i.e* relighting of the images and thus be able to obtain a precise representation of the state of the artwork, which is crucial for documentation purposes. The fourth dataset (dataset RTI-D4 Figure 18d), is a raw flat manufactured metallic surface, treated with blasting and showing some blasting defects. This surface was acquired with the same RTI Dome-based system as dataset RTI-D1. The surface was acquired under 101 different lighting directions and from the dataset surface normals and saliency maps were estimated. Surface characteristics are analyzed following features described by *Nurit et al* [12]. Further analysis and results are presented in the corresponding section.

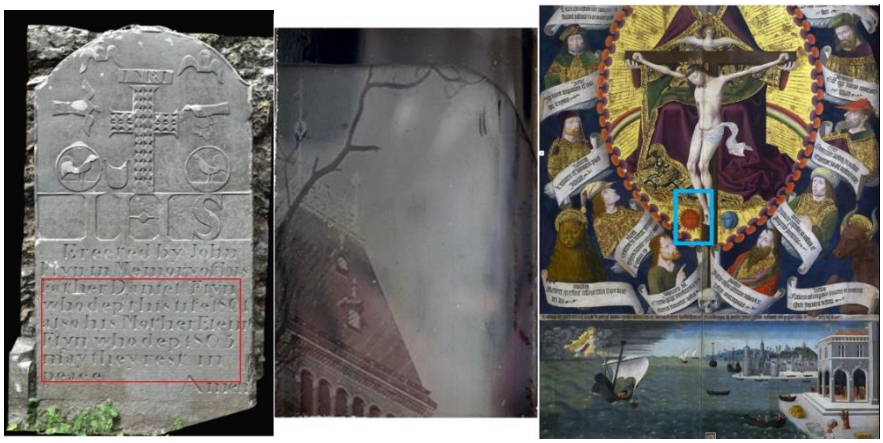

a) headstone (RTI-D1) *b) Daguerreotype (RTI-D2)* *c) Retable de la Trinité (RTI-D3)*

d) Manufactured surface

Fig. 18. Case study samples a headstone, a modern daguerreotype, a historical painting, and a metallic manufactured surface.

5.1 Headstone dataset RTI-D1

The RTI technique has already been used to analyze stone inscriptions; however, in this section, we demonstrate the importance of dealing with non-uniform illumination to improve the visibility of such inscriptions. To do this, we rendered the 3D model of the headstone using 20 lighting directions, then we applied the block of step B1 of the proposed methodology. The results for 3 different angular positions are shown below. Figure 19a, shows the input image for light position $\theta = 185.2°, \phi = 40°$, as it can be notice, the light is coming from the left-side corner, and this area of the surface is brighter. On the contrary, the right side of the surface appears darker in comparison, making the engraving more difficult to read. Figure 19b shows the effect of applying the proposed methodology to the input image; the lighting is more homogenous and the marked contrast between the left and right areas of the surfaces is less prominent, resulting in a better appreciation of the inscription.

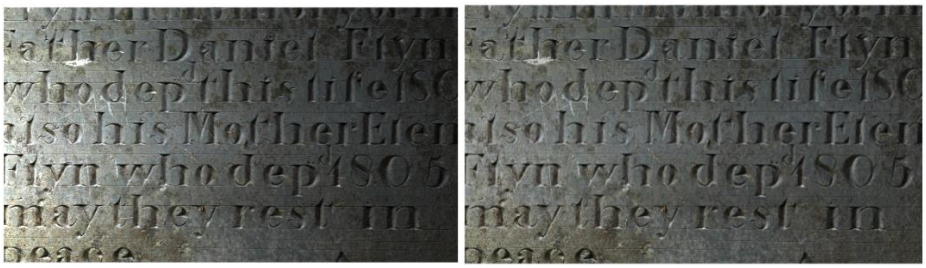

a) Input image *b) Corrected image*

Fig. 19. Correction for input image at light position $\theta = 185.2°, \phi = 40°$.

Similarly, we can see in Figure 16a the image acquired at angular position $\theta = 163°, \phi = 40°$that the light comes from the top-left corner, producing an effect like that seen in the previous image (Figure 19a), making the right side of the surface appear less lighted. The resulting image after employing the proposed methodology is shown in Figure 20b, where the lighting is more uniform. Conversely, in Figure 21b, the result produced after applying the proposed approach to the image corresponding to angular position $\theta = 20°, \phi = 40°$ can be seen (see Figure 21a). Similarly, after applying the correction, the lighting is more uniform, which allows for a better visualization of the inscriptions.

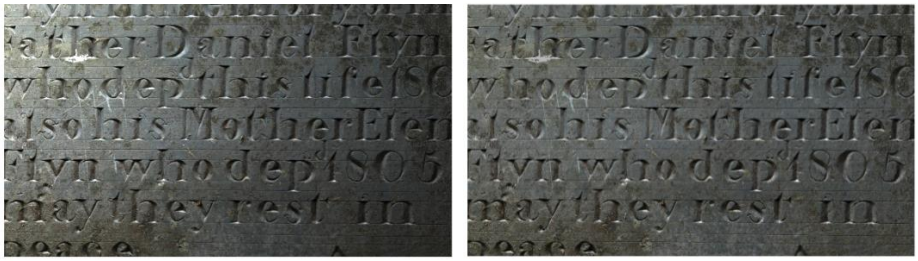

a) Input image *b) Corrected image*

Fig. 20. Correction for input image at light position $\theta = 163°, \phi = 40°$.

a) Input image *b) Corrected image*

Fig. 21. Correction for input image at light position $\theta = 20°, \phi = 40°$.

5.2 Daguerreotype dataset RTI-D2

Being a metallic object, the studied daguerreotype presents a high reflection in angular positions close to the normal. On the contrary, when the surface is illuminated in grazing positions, the reflected light tends to be very little. This behavior generates an important number of saturated pixels in the first case, and in contrast, many poorly illuminated pixels in grazing lighting. Figure 22a shows the input image, which is shown with a false colormap to better appreciate the intensity variation. It can also be noticed some pixels at the center of the image present a high specular reflection producing saturated areas. This behavior emphasizes the defects over the surface, hiding the details of the surface. To overcome this, the second step of the presented method is used. In this case a new image is acquired at the same angular position but using the minimum value of estimated coefficient in order to decrease the exposure time and limit saturation. This produces a so called (I_{min}) image that is used to adjust saturated pixels. Results regarding this applied to the input image can be seen in Figure 22b. It can be observed that the saturation effect is significantly improved thanks to the application of the proposed method. This reduces the effect of the scratches in the surface allowing to better appreciate the details of the building.

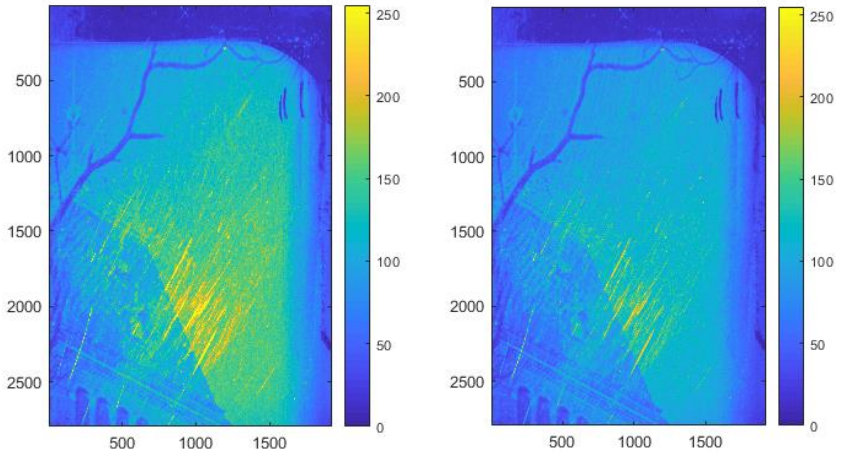

(a) Input image *(b) Adjusted image*

Fig. 22. correction for overlit pixels for input image at $(\theta = 321°, \phi = 69°)$.

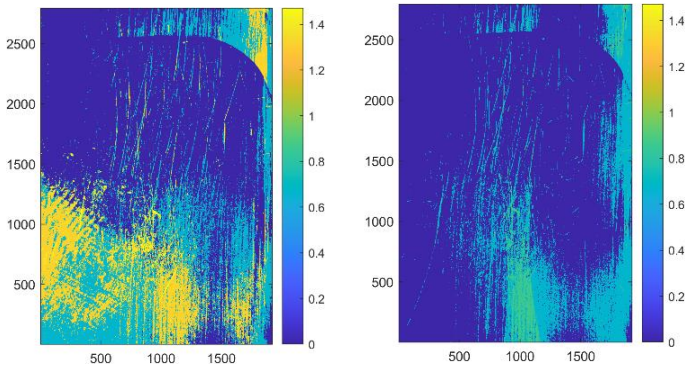

(a) Saturation map before *(b) Saturation map before*

Fig. 23. Comparison of saturation maps for overlit pixels before and after correction.

Using all the images of the dataset, it is possible to estimate the percentage of saturated pixels across all the images, this is done by counting the number of times that a pixel falls into saturation values across the dataset. This let us to produce the "Saturation map". In Figure 23 saturation maps corresponding to the dataset before and after correction are presented. Thanks to these maps it is possible to see that without applying the correction the amount of overlight pixels is higher along all the images of the dataset. On the other hand, it can be appreciated that after applying the correction, the amount of overlit pixel is reduced.

Similarly, in order to manage dark (underexposed) pixels, a solution is presented. Figure 24a, shows the input image acquired at grazing angular position $\theta = 15, \phi = 20$. It can be seen that the building part looks darker, presenting a marked contrast with the

background part. To improve illumination, the proposed method regarding the underlit pixels is applied. Result is shown in Figure 24b. It can be observed that the image is significantly improved thanks to the application of the method, reducing the high contrast between the darkest part of image (building) and the clearest one (background).
We considered overlit as well as undelit pixels not measured points, as these pixels do not really provide information, they are errors due to the surface nature and its interaction with light source that produces either saturation on the captor providing super bright pixels or on the contrary proving dark pixels. In Figure 25a it can be observed the amount of unmeasured information (underexposed and overexposed pixels), according to the angular position. The percentage of unmeasured pixels is higher before applying the proposed method, the population of these pixels is larger in both close to normal, and at grazing positions. On the contrary this percentage is reduced thanks to the used of the method here proposed, as it shows in Figure 25b.

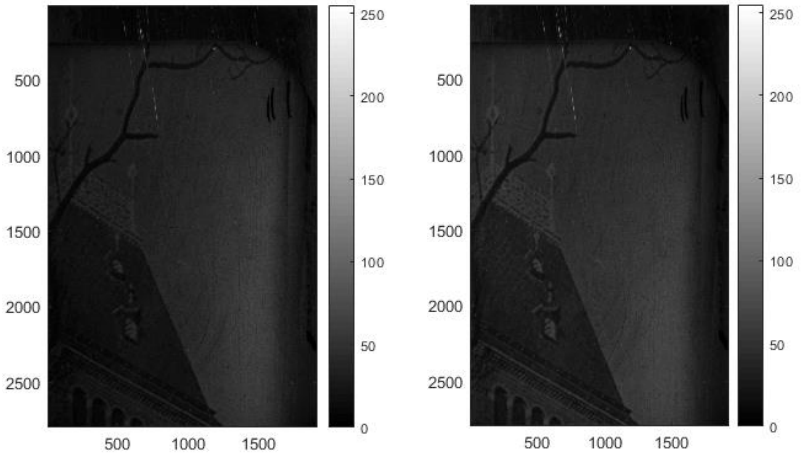

(a) Input image *(b) Adjusted image*

Fig. 24. correction for underlit pixels for input image at $(\theta = 14.9°, \phi = 20°)$.

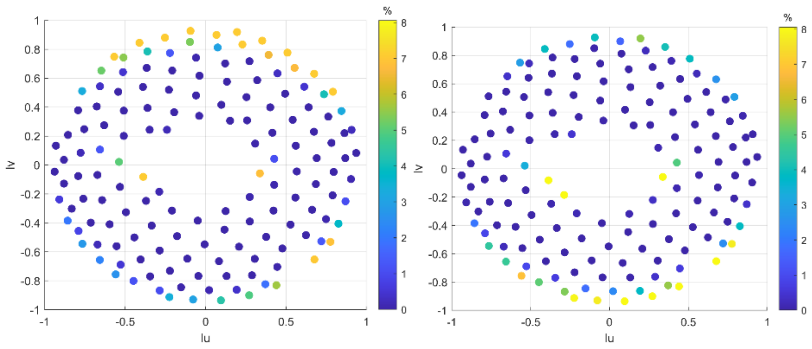

(a) Unmeasured pixels before *(b) Unmeasured pixels after*

Fig. 25. Percentage of unmeasured pixels before and after application of per pixel illumination correction.

5.3 CH surface dataset RTI-D3: application of the angular correction for RTI relighting (Retable de la trinité dataset RTI-D3)

This artwork was processed using the proposed illumination correction. The corrected images were then relight using the HSH approach. Considering this per-pixel angular position correction, it is possible to provide a more accurate reconstruction of the angular reflectance and therefore a better relighting. In Figure 26b, correction regarding only the B1 is presented for input image in Figure 26a, then resulting image after relighting is presented in Figure 26c. In Figure 27 the corrected and corresponding relight image are shown, for a different angular position. From these results, it can be observed that energy corrected images present a more uniform lighting. Furthermore, as the per-pixel corrected angular position is used to model the surface, the reconstructed image is also improved. The proposed method can be applied independently of the RTI modeling approach that is used to relight the surface.

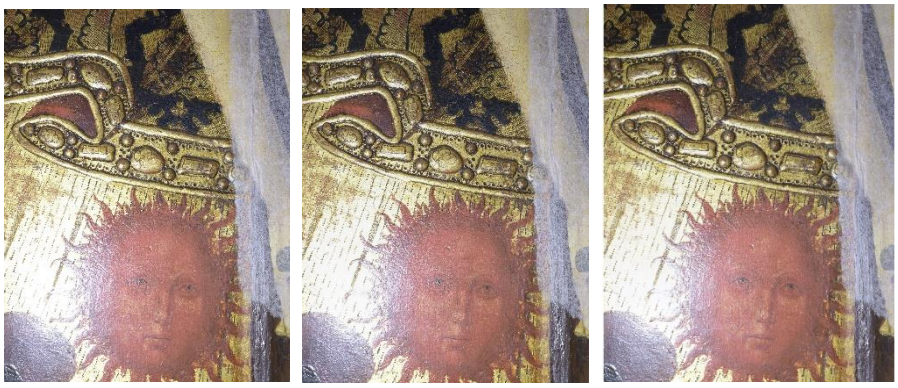

a) Input Image *b) I_{B1} corrected Im* *c) I_{B1} corrected Im relighted*

Fig 26. Relight image at light position $\theta = 220°$, $\phi = 80°$.

a) Input Image *b) I_{B1} corrected Im* *c) I_{B1} corrected Im relighted*

Fig 27. Relight image at light position θ = 160°, ϕ = 65°.

5.4 Manufactured surface dataset RTI-D4

Here we present the proposed correction method applied to a metallic industrially manufactured surface. This surface presents characteristics that allow us to show the efficiency of the method. In the lower right corner, an engraving is observed in the surface. This feature is used to evaluates the correction performed by the method regarding the saliency (saliency maps offer information on the notable local characteristics of a surface [28, 29]). Saliency maps before (Figure 28a) and after (Figure 28b) the application of the proposed per-pixel processing method are presented.

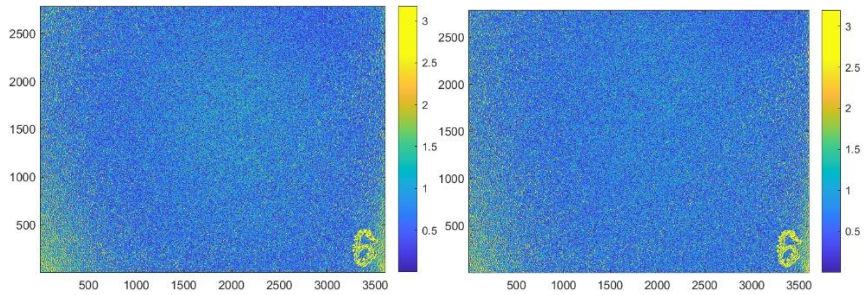

(a) Saliency map before *(b) Saliency map after*

Fig. 28. Saliency maps for manufactured surface before and after applying the proposed methodology.

As it can be seen in the Figure 30a where the difference between both the adjusted and not adjusted saliency map is presented, the engraved number appears more visible on the adjusted saliency map (Figure 28b). On the other hand, pixels at the center of the surface seems less salient as they the geometry of this part of the surface is more like the one presented by pixels at the surface borders. Considering the elevation angle (ϕ), as a geometrical descriptor (as described by [29], geometrical descriptors allow to

analyze the surface micro-geometry (topography) through information derived from the normal maps), it can be observed at Figure 30b, the difference between the resulting ϕ angle of the normal maps (normal map with (Figure 29a) and without (Figure 29b) proposed method). From this difference map, we can observe that, higher variation is presented at the borders, as in the pixels closer to center differences are lower. This behavior is consistence with the described problem. As the rays spread from the center, the angle of every ray changes.

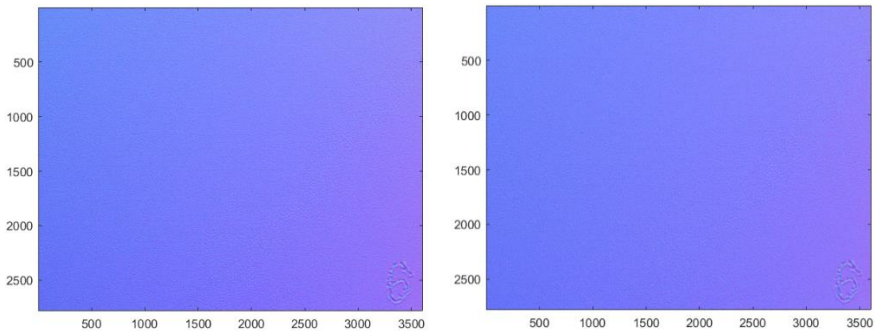

(a) Normal map before *(b) Normal map after*

Fig. 29. Difference between corrected and not corrected normal maps and Difference between corrected and not corrected saliency maps.

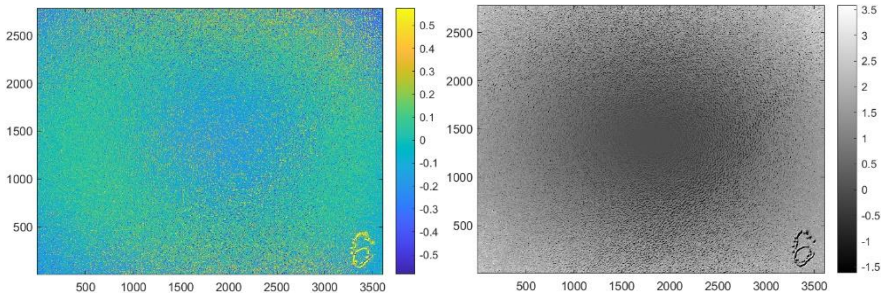

(a) Difference between saliency maps *(b) Difference between normal maps*

Fig. 30. Difference between corrected and not corrected normal maps and Difference between corrected and not corrected saliency maps.

6 Conclusion

This paper proposed a methodology to palliate the nonuniform illumination obtained with non-collimated light sources performing RTI acquisitions. We show that it is possible to obtain a per-pixel estimation of light-surface distance as well as light angular position knowing the real size of the surface as well as the light distance and angle at

the center of the surface. We also provide evidence that, using the estimated distances and the elevation angles, it is possible to obtain adjustment coefficients following the illumination model of a point light source. Results provided here confirm that when the proposed per-pixel modeling method is applied, images present an improvement regarding the illumination uniformity. The proposed methodology also offers the advantage of obtaining the angular position per pixel, which distinguishes it from the traditional RTI method where a single angular position is applied to the entire surface. This pixel-wise angular information, captured in the LP file, enables a more accurate and precise reconstruction of surface features. Finally, we can conclude that the incorporation of per-pixel adjustments for both the perceived illumination and angular position yields significant improvements in visualizing surface features. This approach enhances the reliability and accuracy of the information obtained, offering a more comprehensive understanding of the surface's condition.

7 Discussion and Future work

In this work, we have conducted a study of the illumination variation observed in RTI and other multi-light approaches. This variation arises due to the utilization of non-collimated light sources. It is important to note that achieving a perfectly modeled distant light source is not feasible under the conditions in which these acquisitions take place. Therefore, although the proposed method helps to mitigate the effects caused by non-uniform illumination, there are still more issues to be resolved. While the proposed methodology, especially part B2, can improve cases where there are unmeasured pixels (over- or under-exposed), the impact of the result may be diminished on very heterogeneous surfaces. For example, in the case of a surface that has both glossy and matte areas, it will be difficult to find a balance between the illumination and the respective correction applied to properly visualize the surface. Likewise, the B2 part of our method is limited to the use of a suitable acquisition system. Since in the case of using a hand-held light, it is difficult to take a second and/or third image while maintaining the same angular position.
In future work and with the idea of further improving the proposed method, it is important to investigate, the distance between the surface and the lamp, which in hand-held light acquisition (H-RTI) is not always consistent among the acquired images. The fluctuation of this distance is crucial because it changes the amount of light emitted towards the surface of light emitted towards the surface, resulting in inconsistent illumination in a series of RTI images.

8 Acknowledgements

This work benefited of the funding of French National Research Agency (ANR) through the project CE38-004 SUMUM (www.anr-sumum.fr). Authors also thanks the Rijks Museum for providing the modern daguerreotype.

9 Data Availability

One of the datasets analyzed during this study (headstone from Monsea church) is available online and the 3D model can be download from SketchFab (https://sketchfab.com) under a creative commons attribution license. The other datasets used in this work are not public and are the property of the authors of this publication.

10 Conflict of interest

There are no conflicts of interest concerned with this article and there were no experiments conducted using subjects of any kind.

References

1. Earl, G., Basford, P., Bischoff, A., Bowman, A., Crowther, C., Dahl, J., Hodgson, M., Isaksen, L., Kotoula, E., Martinez, K., et al., 2011. Reflectance transformation imaging systems for ancient documentary artefacts. Electronic Visualisation and the Arts (EVA) , 147–154 (2011).
2. Einarsson, P., Hawkins, T., Debevec, P. Photometric stereo for archeological inscriptions, in: ACM SIGGRAPH Sketches, 81 (2004).
3. Gautron, P., Krivanek, J., Pattanaik, S.N., Bouatouch, K.. A novel hemispherical basis for accurate and efficient rendering. Rendering Techniques. 321–330 (2004).
4. Giachetti, A., Ciortan, I.M., Daffara, C., Marchioro, G., Pintus, R., Gobbetti, E. A novel framework for highlight reflectance transformation imaging. Computer Vision and Image Understanding. 168, 118–131 (2018).
5. Ikeuchi, K. Determining surface orientation of specular surfaces by using the photometric stereo method. Pattern Analysis and Machine Intelligence, IEEE Transactions on Pattern Analysis and Machine Intelligence, 661 – 669. doi:10.1109/TPAMI. 1981.4767167.
6. Lam, P.M., Leung, C.S., Wong, T.T., 2012. Noise-resistant hemispherical basis for image-based relighting. Image Processing, IET 6, 72–86. doi:10.1049/iet-ipr.2009.0134.
7. MacDonald, L. Visual realism in digital heritage, in: Heritage Preservation (2018).
8. Malzbender, T., Gelb, D., Wolters, H. Polynomial texture maps. Proceedings of the 28th annual conference on Computer graphics and interactive techniques, 519–528 (2001).
9. Masselus, V., Dutré, P., Anrys, F. The free-form light stage, in: ACM SIGGRAPH 2002 conference abstracts and applications, pp. 262–262 (2022).
10. McGuigan, M., Christmas J. Automating rti: Automatic light direction detection and correcting non-uniform lighting for more accurate surface normals, in: Computer Vision and Image Understanding, University of Exeter, Exeter, EX4 4QF, UK. p. 102880 (2020).
11. Mudge, M., Malzbender, T., Schroer, C., Lum, M. New reflection transformation imaging methods for rock art and multiple-viewpoint display, in: Ioannides, M.; Arnold, D.; Niccolucci, F. & Mania, K., eds., The 7th International Symposium on Virtual Reality, Archaeology and Cultural Heritage, Vast. pp. 195–202 (2006).
12. Nurit, M., Le Goïc, G., Lewis, D., Castro, Y., Zendagui, A., Chatoux, H., Favrelière, H., Maniglier, S., Jochum, P., Mansouri, A. Hd-rti: An adaptive multi-light imaging approach for the quality assessment of manufactured surfaces. Computers in Industry 132, 103500 (2021).

13. Pamart, A., Ponchio, F., Abergel, V., Mamp;apos;Darhri, A., Corsini, M., Dellepiane, M., Morlet, F., Scopigno, R., Luca, L. A complete framework operating spatially-oriented rti in a 3d/2d cultural heritage documentation and analysis tool. ISPRS - International Archives of the Photogrammetry, Remote Sensing and Spatial Information Sciences XLII-2/W9, 573–580 (2019).
14. Pintus, R., Dulecha, T.G., Ciortan, I., Gobbetti, E., Giachetti, A. State-of-the-art in multi-light image collections for surface visualization and analysis, in: Computer Graphics Forum 2019. The Eurographics Association and John, Department of Computer Science, University of Verona, Italy; Norwegian University of Science and Technology, Department of Computer Science, Norway. p. 3 (2019).
15. Pitard, G., Le Goic, G., Mansouri, A., Favreliere, H., Désage, S.F., Samper, S., Pillet, M. Discrete Modal Decomposition: a new approach for the reflectance modeling and rendering of real surfaces. Machine Vision and Applications 28, 607–621 (2017).
16. Rabascall, I. Uncalibrated photometric stereo for 3 d surface texture recovery (2003).
17. Tunwattanapong, B., Fyffe, G., Graham, P., Busch, J., Yu, X., Ghosh, A., Debevec, P. Acquiring reflectance and shape from continuous spherical harmonic illumination. ACM Transactions on graphics (TOG) 32, 1–12 (2013).
18. Walton, M., Cossairt, O., Huang, X., Bearman, G. Near light correction for image relighting and 3d shape recovery (2015). doi:10.1109/DigitalHeritage.2015.7413874 .
19. Winnemoeller, H., Mohan, A., Tumblin, J. Light waving: Estimating light positions from photographs alone. Comput. Graph. Forum 24, 433–438 (2005). doi:10.1145/1187112.1187164 .
20. Woodham, R.J. Photometric method for determining surface orientation from multiple images. Optical engineering *19*(1), 139-144. (1980.)
21. Luxman, R.; Castro, Y. E.; Chatoux, H.; Nurit, M.; Siatou, A.; LeGoïc, G.; Brambilla, L.; Degrigny, C.; Marzani, F.; Mansouri, A. LightBot: A Multi-Light Position Robotic Acquisition System for Adaptive Capturing of Cultural Heritage Surfaces. J. Imaging 8, 134 (2022).
22. Kratky, V., Petracek, P., Spurny, V. et Saska, M. Autonomous reflectance transformation imaging by a team of unmanned aerial vehicles. IEEE Robotics and Automation Letters, vol. 5, no. 2, pages 2302–2309, (2020).
23. Ponchio, F., Corsini, M., & Scopigno, R. A compact representation of relightable images for the web. In Proceedings of the 23rd International ACM Conference on 3D Web Technology pp. 1-10 (2022).
24. Iwahori, Y., Sugie, H., & Ishii, N. Reconstructing shape from shading images under point light source illumination. In Proceedings. 10th International Conference on Pattern Recognition Vol. 1, pp. 83-87. IEEE (1990).
25. Quéau, Y., Durix, B., Wu, T., Cremers, D., Lauze, F., & Durou, J. D. Led-based photometric stereo: Modeling, calibration and numerical solution. *Journal of Mathematical Imaging and Vision*, *60*(3), 313-340 (2018).
26. Santo, H., Waechter, M., & Matsushita, Y. Deep near-light photometric stereo for spatially varying reflectances. In European Conference on Computer Vision pp. 137-152. Springer, Cham (2018).
27. Dulecha, T. G., Fanni, F. A., Ponchio, F., Pellacini, F., & Giachetti, A. Neural reflectance transformation imaging. *The Visual Computer*, *36*(10), 2161-2174 (2020).
28. Pitard, G., Le Goïc, G., Mansouri, A., Favrelière, H., Pillet, M., George, S., & Hardeberg, J. Y. Reflectance-based surface saliency. In *2017 IEEE International Conference on Image Processing (ICIP)* (pp. 445-449). IEEE (2017).

29. Nurit, M., Le Goïc, G., Maniglier, S., Jochum, P., Chatoux, H., & Mansouri, A. Improved visual saliency estimation on manufactured surfaces using high-dynamic reflectance transformation imaging. In *Fifteenth International Conference on Quality Control by Artificial Vision* (Vol. 11794, pp. 111-121). SPIE (2021).
30. Murat, K. U. R. T. A survey of BSDF measurements and representations. *Journal of Science and Engineering*, *20*(58), 87-102 (2018).
31. Kurt, M., & Edwards, D. A survey of BRDF models for computer graphics. *ACM SIGGRAPH Computer Graphics*, *43*(2), 1-7 (2009).
32. Tongbuasirilai, T., Unger, J., Kronander, J., & Kurt, M. Compact and intuitive data-driven BRDF models. *The Visual Computer*, *36*, 855-872 (2020).
33. Castro, Y., Nurit, M., Pitard, G., Zendagui, A., Le Goïc, G., Brost, V., ... & De Luca, L. Calibration of spatial distribution of light sources in reflectance transformation imaging based on adaptive local density estimation. *Journal of Electronic Imaging*, *29*(4), 041004-041004 (2020).